Journal of Astronomical Instrumentation

Cosmic Dawn Intensity Mapper: Spacecraft and Mission Design for a Probe-Class Space Telescope

Philip Linden[1,†], Michael Zemcov[2]
[1] *Department of Mechanical Engineering, Kate Gleason College of Engineering, Rochester Institute of Technology, Rochester, NY 14623, USA, pjl7651@rit.edu*
[2] *Center for Detectors, School of Physics and Astronomy, Rochester Institute of Technology, Rochester, NY 14623, USA, zemcov@cfd.rit.edu*

Received (to be inserted by publisher); Revised (to be inserted by publisher); Accepted (to be inserted by publisher);

Cosmic Dawn Intensity Mapper (CDIM) is a Probe-class near-IR space telescope with the scientific goal of conducting large spectro-imaging surveys over a five-year mission in the next decade. A high-level system architecture was designed to identify key features and technologies aboard the CDIM spacecraft in preparation for future detailed design studies.

Keywords: spacecraft, telescope, system, cryogenic, infrared, design.

1. Introduction

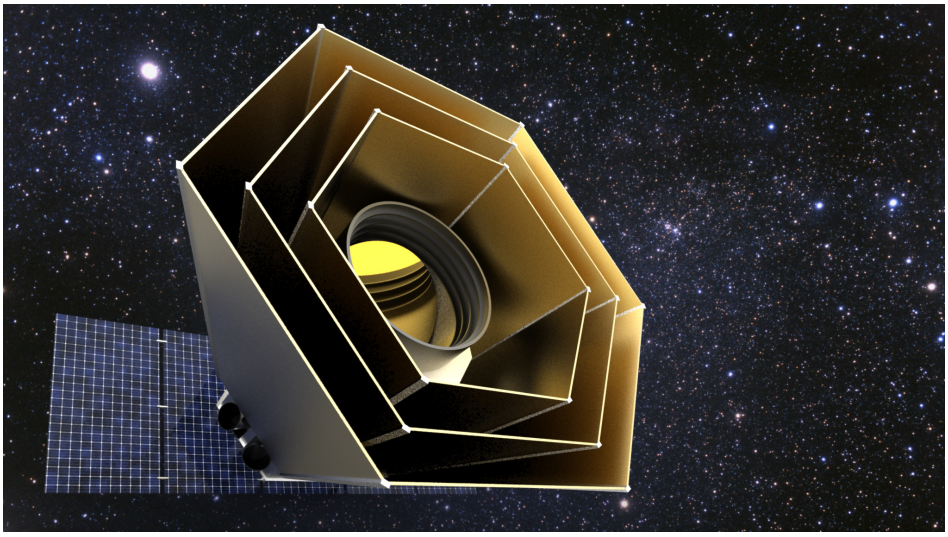

Fig. 1. An artistic rendition of the Cosmic Dawn Intensity Mapper stationed at Sun-Earth L_2.

The Cosmic Dawn Intensity Mapper (CDIM) is a concept for a Probe-class 1.5 m aperture telescope, passively cooled to 45 K, with an actively cooled 6×6 detector array that utilizes linear variable filters (LVFs) (Cooray *et al.*, 2016) capable of three-dimensional spectro-imaging observations over the wavelength range of 0.75 to 7.5 µm at a spectral resolving power R= 500. CDIM has a 10 $\deg^2$ instantaneous field of

†Corresponding author.

Table 1. Critical design requirements for the CDIM spacecraft.

Spacecraft Design Driver	Impact	Target
Cost	Science capability, instrument architecture	less than \$1 B
Mass	Launch vehicle	less than 1000 kg
Temperature (OTA)	Passive radiator	45 K
Temperature (Detector)	Cryocooler	35 K
Pointing Requirements	Attitude control system	less than 0.5 arcsec
Lifetime	Redundancy, RCS propellant	5 years
Orbit	Solar array, thermal management, launch vehicle, telemetry	Sun-Earth L_2

view (FoV) atop a focal plane of thirty-six 2048×2048 detectors. The survey strategy using spacecraft operations following a shift and stare mode will result in 1360 independent narrow-band spectral images of the sky on a given location. Surveys are planned to span from $25\,\mathrm{deg}^2$ up to $1000\,\mathrm{deg}^2$ over a five year lifetime in an orbit about Sun-Earth Lagrange point L_2.

Although Wide Field Infrared Survey Telescope (WFIRST) will be capable of $3400\,\mathrm{deg}^2$ wide area surveys, its spectroscopy is limited to 2 µm, limiting the selection of galaxies it is able to observe (Green *et al.*, 2012). While James Webb Space Telescope (JWST) is capable of targeted spectroscopy studies of galaxies present in reionization and surveys $10\,\mathrm{armin}^2$ for reionization galaxies (Gardner *et al.*, 2006), CDIM will make use of tomographic intensity mapping of spectral emission lines to study the aggregate statistical properties of the sources and their spatial distribution. The intensity of the Lyα and Hα lines, combined with others, will also provide critical clues to the formation of metals in the universe (Cooray *et al.*, 2016).

Probe-class missions occupy a role on a larger scale than Discovery missions, such as Kepler and Dawn, but not as large as Flagship missions such as JWST. Such missions are intended to be PI-led scientific investigations rather than general observatories, and have a firm \$1B cap (Wiseman *et al.*, 2015). Critical design requirements to achieve CDIM's science goals as a Probe-class mission are summarized in Table 1. CDIM will leverage mature and flight-proven technology to reduce development costs.

2. Optical Telescope Assembly

Preliminary explorations indicate that a 1.3–1.5m aperture off-axis primary mirror cooled to 45 K is required to meet CDIM's spectro-imaging requirements (Cooray *et al.*, 2016). The primary mirror is notionally assumed to be constructed from light-weighted Corning (ultra-low expansion) silica-titania glass with a honeycomb core and a gold-deposition surface coating. For this type of mirror, the estimated mass is in the neighborhood of 200 kg.

For near-IR observations, the primary mirror must be cooled to cryogenic temperatures. Rather than including a heating element and detectors that operate at warm temperatures, it is advantageous to use detectors that operate at cryogenic temperatures as well so as to minimize thermal radiation that could be detrimental to near-infrared (near-IR) observations.

A 6×6 array of 2048×2048 pixel detectors is required cover a $10\,\mathrm{deg}^2$ focal plane with 1 arcsec pixels. HgCdTe infrared detectors meet CDIM design goals of operating at cryogenic temperatures, low in cost, and, of course, sensitive in near-IR. Several types of HgCdTe detectors satisfy CDIM's spatial resolution, wavelength range, and sensitivity requirements. These detectors range in technology-readiness-level (TRL), but all are sufficiently developed to be considered for the 2020 Decadal and will be demonstrated on missions such as NEOCam, SPHEREx, and JWST (Doré *et al.*, 2014; Gardner *et al.*, 2006). Candidate detectors are listed in Table 2.

CDIM will utilize 36 detectors in a close-packed, 6×6 mosaic focal plane assembly (FPA). In the expected normal operating mode, each detector dissipates less than 4 mW, for a total power dissipation of less than 150 mW for the full array.

Linear-variable filters (LVFs) will be placed just above the detectors to provide spectral dispersion for spectrometry. LVFs are precision-coated optical filters with spectral properties that vary linearly across the length of the filter, which provide high transmissibility for narrow bandwidths and deep blocking of unwanted light. Figure 2 shows how LVFs may be arranged in conjunction with CDIM's detector array.

Table 2. Candidate Teledyne 2048 × 2048 pixel detectors for the CDIM FPA.

	TRL	Wavelength Range	Heritage
HyVisi	4	0.5–0.8µm	1024 × 1024 (TRL 9)
H2RG-2.5	8	0.9–2.5µm	1024 × 1024 (TRL 9)
H2RG-5.0	8	2.5–5.0µm	1024 × 1024 (TRL 9)
H2RG-8.0	4	5.0–10.0µm	1024 × 1024 (TRL 6)

LVFs are simple, space-qualified solutions to permit spectral data cubes between 0.75–7.5µm that are commercially available and significantly lower in cost than more complex systems (Turner *et al.*, 2016).

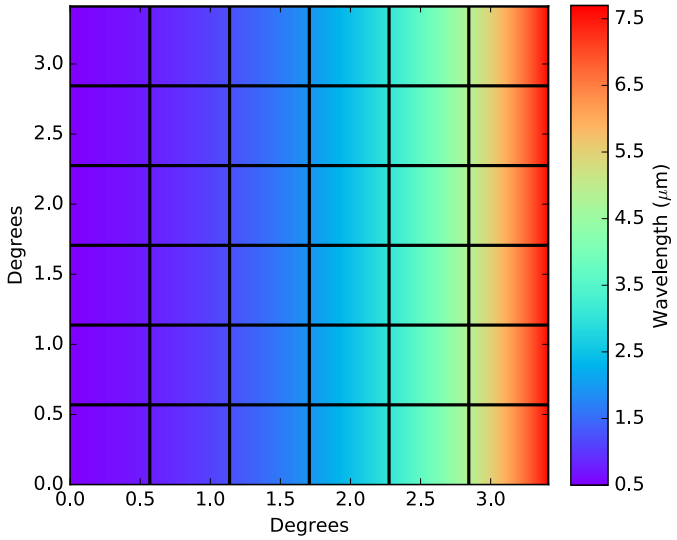

Fig. 2. A possible arrangement of linear-variable filters with a 6 × 6 detector array.

CDIM optics, instruments, and focal plane will be housed in an aluminum light-tight box that is be bead blasted to a matte finish and black anodized. The purpose of this housing is to reduce reflections and scattered light from the exposed, reflective portions of the detectors.

The optical telescope assembly (OTA) as a whole is estimated to have a mass of 200–250kg.

3. Thermal Design

CDIM will employ both passive and active thermal regulation systems. By using passive radiators in tandem with an active cryocooler, the static OTA heat load can be dissipated by the lightweight radiator and a smaller cryocooler may be used to only cool the detector array rather than the whole OTA mass plus FPA. Passive cooling is used to cool the OTA and FPA from solar radiation, while active cooling regulates heat dissipated by active detectors.

The OTA is cooled to 45 K to reduce background photon load in the near-IR. Passive thermal regulation is maintained using a multi-stage V-groove radiator, which bounces radiative heat into the 3 K background of space (Bard, 1987). V-groove radiators have been demonstrated in passive cryogenic radiators down to 4 K with Planck, SPIRIT, and Spitzer (warm mission). In order to achieve passive cooling from a baseline temperature of 300 K at Sun-Earth Lagrange point L_2, CDIM will feature a multi-stage V-groove radiator. Since CDIM may be at various angles of incidence to solar radiation as it surveys the sky, the V-groove radiator vanes will "umbrella" outward. This way, the radiator cools the OTA at any attitude facing away from the sun.

The first, sun-facing stage of the radiator is thin-walled, highly reflective, and low-emissive material which rejects most of the solar radiation by reflection. Thermal radiation is emitted by the first stage and

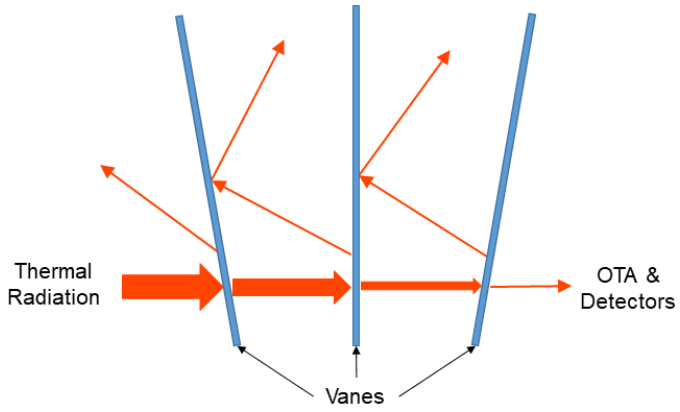

Fig. 3. Low emmissivity, high specular surface vanes are nested at a slight angle to reflect thermal radiation into space, cooling the OTA to 45 K. (Rasbach, 1988) A mechanical cryocooler cools the FPA to 35 K.

again reflected to space by subsequent stages (Gilmore & Donabedian, 2003).

The solution to achieve 45 K at the OTA is not unique, and parameters such as radiator materials, surface finishes and coatings, relative angle, separation, and area may be adjusted accordingly. To explore this design space, detailed parametric and finite-element analyses exist (Couto *et al.*, 2002; Morgante *et al.*, 2015) but are not discussed here.

CDIM's thermal requirement to reduce thermal noise in the detector array can be met by actively cooling the array to 35 K by a mechanical cryocooler. Stirling-cycle mechanical refrigerators are low-vibration, high-reliability, and lightweight active cryocooling systems that have significant heritage in space applications. Pulse-tube mechanical cryocoolers are similar to Stirling cryocoolers in capacity, cost, and function. While Stirling cryocoolers use mechanisms to drive the thermodynamic cycle, Pulse-tube cryocoolers use an acoustic standing wave. Either type of cryocooler is suitible for CDIM, and both types have significant heritage in space applications (Gilmore & Donabedian, 2003). One candidate system is Raytheon's PSC 1-stage Stirling cryocooler, capable of cooling a 1.2 W parasitic heat load to 35 K. This cryocooler is 18.6 kg and requires 88 W of input power (Ross, 2005).

In this configuration, the most significant heat loads from the cooled section come from conduction through the OTA support structure, which isolates the cooled section from the warm spacecraft bus. Only the mirror and detectors need to be cooled to cryogenic temperatures. Electronics boards that control the FPA and instrumentation need not be cryocooled. These warm electronics are housed in CDIM's spacecraft bus with other spacecraft systems. Some components that require cooling below the temperature of the bus, but not so far as the FPA, may be placed between stages of the V-groove radiator. The back side of CDIM's solar array acts as a radiator to thermally regulate the spacecraft bus. A notional map of heat transfer is shown in Figure 4.

4. Attitude Determination and Control

CDIM will be three-axis stabilized using an inertial reference unit and star-trackers. Star trackers identify constellations in their field of view to determine the spacecraft's attitude to within 1–3 arcseconds. These systems are used to coarsely slew CDIM to a target.

Rather than using more accurate (and more expensive) inertial or star-tracking sensors, fine pointing guidance sensors may be included on the focal plane, as demonstrated by WFIRST (Green *et al.*, 2012). These fine guidance sensors enable CDIM to meet its relative pointing control requiremend of 2.5 arcsec. Redundant systems are included to allow CDIM to operate in different power states. Low-fidelity attitude determination sensors such as sun sensors are cheap, accurate to less than one degree, and lightweight. Sun sensors provide CDIM with a coarse safe-hold capability.

In a heliocentric orbit, the primary disturbance to the spacecraft's attitude is solar radiation pressure (SRP). Solar radiation pressure imparts a near-constant 4.5e−10 $\mathrm{N\,m^{-2}}$ to spacecraft orbiting $\mathrm{L_2}$ (Evans *et al.*, 2002).

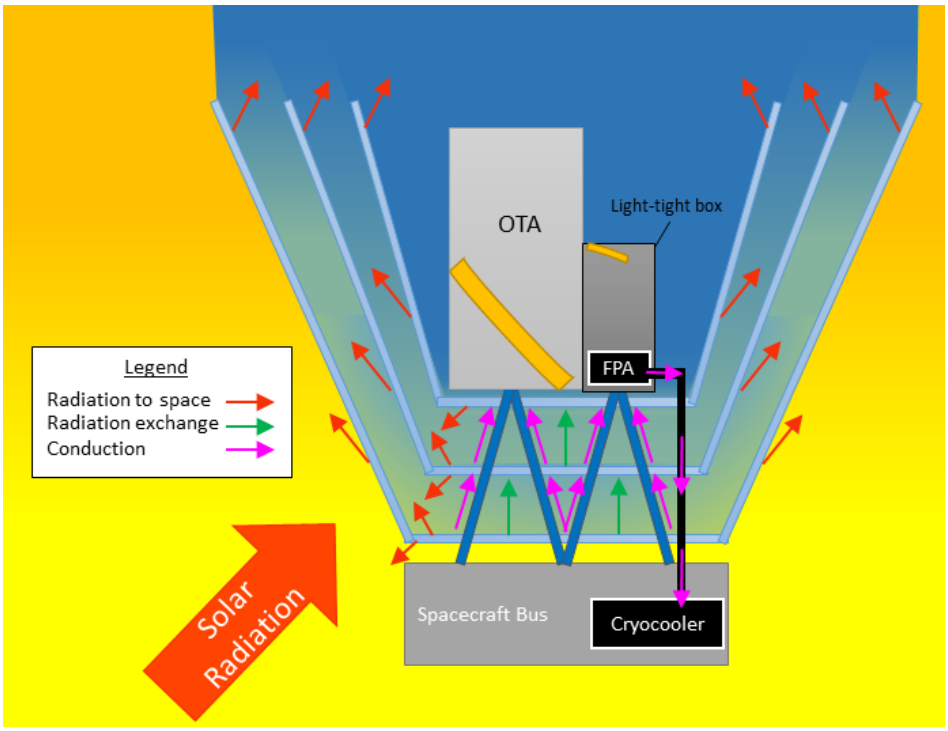

Fig. 4. Notional pathways and heat loads throughout the cooled section are shown (not to scale).

Hydrazine monopropellant thrusters will be used for orbit station-keeping as well as momentum management. A desired attitude is maintained by the spacecraft using a 3-axis zero-momentum inertial system, whereby the error in attitude due to SRP is cancelled out by spinning up or slowing down reaction wheels. Reaction wheel systems are capable of torques ranging from .01 to 1N m and store 0.4 to 3000N m s of practical momentum (Wertz *et al.*, 2015). Power consumption varies with reaction wheel speed, with a maximum estimate of roughly 100 W. After some time the inertial attitude control may become saturated. Desaturation is managed by engaging station-keeping thrusters for short periods of time. Additionally, these thrusters will be used to maintain an orbit at L_2 as it is an inherently unstable orbit.

5. Flight Computer

CDIM will be capable of autonomous operation and system diagnostics. Nominal operation includes maintaining a attitude during imaging, slewing across the sky to conduct a survey, capturing images, and downlinking data to Earth. Images will be processed on-board CDIM using an algorithm demonstrated by SPHEREx (Zemcov *et al.*, 2016).

6. Telemetry

Typically for high-Earth and deep-space missions, the X-Band Space Science frequency band is used for uplink and downlink between the spacecraft and Ground Stations. Thus, high-gain antennas are best suited for both links (Wertz *et al.*, 2015).

The data rate and data volume generated by a CDIM survey is estimated by scaling the known performance of SPHEREx. A survey conducted by SPHEREx using four 2048 × 2048 H2RG detectors generates araw data volume, D, of 168.39 Gbit/day, and uses on-board processing that compresses the data at a compression ratio of 2.5:1 before downlinking, resulting in a final data volume, D_c of 63.7 Gb/day (Zemcov *et al.*, 2016).

CDIM will use 36 2048 × 2048 detectors and a similar compression algorithm to SPHEREx. The data

volume for CDIM is estimated to be:

$$\begin{aligned} D &= \frac{36}{4}(168.39\,\text{Gbit/day}) \\ &= 1515.5\,\text{Gb/day} \end{aligned} \tag{1}$$

$$\begin{aligned} D_c &= \frac{1}{2.5}(1515.5\,\text{Gb/day}) \\ &= 606.2\,\text{Gb/day} \\ &= 7.0\,\text{Mb/s} \end{aligned} \tag{2}$$

Transmission rates are dependent on the total time available for CDIM to send data to a ground station. For example, the spacecraft could transmit continuously at a very low transfer rate, or send larger volumes of data once per day over 1 hour at the expense of a higher transfer rate.

$$\begin{aligned} D_c &= 606.2\,\text{Gb/hr} \\ &= (606.2\,\text{Gb/hr})(\frac{1\,\text{hr}}{3600\,\text{s}}) = 0.1684\,\text{Gb/s} \\ &= 168.4\,\text{Mb/s} \end{aligned} \tag{3}$$

For redundancy, CDIM is outfitted with multiple communication modes outline in Table 3.

Table 3. Downlink transfer rates reflect estitmates based on the target of 606.2 Gb/day. Typical data transfer rates are outlined for uplinks (Wertz *et al.*, 2015).

Mode	Uplink	Downlink
Emergency	7.8 bps	5–10bps
Engineering data	15.6–2000kbps	Up to 10 bps
Science data	15.6–2000kbps	7.0 Mbps (continuous) or 168.4 Mbps (1 hour per day)

Uplinks will follow standard protocols and do not require transmitting large volumes or particularly fast transfer rates. The CDIM telemetry system, including antenna and power converter, are estimated to have a mass of 2 kg.

7. Power

Since CDIM will be located at L_2, it is exposed to 1291–1421W m^{-2} solar flux (Evans *et al.*, 2002), accounting for Earth's eccentricity and solar flares. All power generation will come from anarray of triple junction Arsenide (GaAs) photovoltaic cells facing the sun. Triple junction GaAs cells are more costly than silicon cells, but are more efficient. An array GaAs cells is more resilient to radiation and will experience less degradation over time compared to silicon cells, which is desirable for CDIM's 5 year mission lifetime.

As CDIM surveys the sky, its angle of incidence to the Sun changes. To maintain sufficient power over the full viewing range, a fixed array must be mounted at an angle, θ, with respect to CDIM's viewing axis. In this configuration, the angle of the array may be optimized such that the power efficiency is maximized in the regions that are most critical for CDIM's science objectives. Alternatively, CDIM could use arrays that are capable of adjusting their angle of incidence to maintain maximum efficiency. For a conservative estimate, it is assumed that the solar array is at 30° from normal to the Sun.

Solar cell efficiency degrades over time from use and radiation. The end-of-life efficieny, η_{EOL} is found with respect to mission duration, L, and estimated efficiency degradation, D (Wertz *et al.*, 2015). For triple junction GaAs cells, D is assumed to be 3% per year.

$$\eta_{EOL} = (1 - D)^L \tag{4}$$

Table 4. Typical efficiencies and margins for a triple junction Gallium Arsenide solar array (Wertz *et al.*, 2015).

Efficiencies			Margins		
Ideal Conversion Efficiency	η_i	33.8%	New Design	m_d	5%
Production Unit Efficiency (with respect to ideal)	η_p	72.0%	Reserves	m_r	20%
Incident Angle (30°)	η_θ	86.6%	Harness Losses	m_h	5%
End of Life (5 year mission)	η_{EOL}	85.9%	Power Regulation Losses	m_p	20%

To be conservative, the solar flux at L_2, P_{sol}, is estimated to be $1291\,\mathrm{W\,m^{-2}}$ (Evans *et al.*, 2002). A similarly conservative estimate of 1200 W is the assumed power draw from all CDIM instruments and components, P_{sc}. CDIM power draw is estimated from the known power draw for WFIRST, as it is a fairly similar spacecraft to CDIM (Green *et al.*, 2012). A summary of margins and efficiencies is listed in Table 4.

The total power the array must supply to the spacecraft is found by summing all power margins:

$$M = m_d + m_r + m_h + m_p = .05 + .2 + .05 + .2 \tag{5}$$

$$P_{sa} = \frac{P_{sc}}{M} = \frac{1200\,\mathrm{W}}{0.50} = 2400\,\mathrm{W} \tag{6}$$

The required solar array area, A_{sa} is determined from the estimated end-of-life power capacity of the array per unit area, P_{EOL}.

$$P_o = P_{sol}\eta_i = (1291\,\mathrm{W\,m^{-2}})(.338) = 436.4\,\mathrm{W\,m^{-2}} \tag{7}$$

$$P_{BOL} = P_o\eta_p\eta_\theta = (436.4\,\mathrm{W\,m^{-2}})(.72)(.866) = 272.1\,\mathrm{W\,m^{-2}} \tag{8}$$

$$P_{EOL} = P_{BOL}\eta_{EOL} = (272.1\,\mathrm{W\,m^{-2}})(.859) = 233.6\,\mathrm{W\,m^{-2}} \tag{9}$$

$$A_{sa} = \frac{P_{sa}}{P_{EOL}} = \frac{2400\,\mathrm{W}}{233.6\,\mathrm{W\,m^{-2}}} = 10.27\,\mathrm{m^2} \tag{10}$$

The $10\,\mathrm{m^2}$ array will be a deployable mechanism, whether or not it is capable of articulating its angle of incidence. Deployable solar arrays are not novel technology so no significant development is anticipated for this subsystem.

The solar array size estimate derived from Equation 7 is fairly conservative. The accuracy of the array size would be much improved if a more accurate estimate of power draw was known.

8. Structure

The mirror and detectors will be supported by low-moisture composites to provide adequate structure stiffness while minimizing mass and conductive heat loads to the cooled section.

The spacecraft bus will be a graphite epoxy composite hexagonal structure, which houses all non-instrumentation systems including the cryocooler, ADCS, telemetry, processing, power modules, and propulsion tank. The bus will also provide hard points for integration with the launch vehicle.

9. Orbit

CDIM will orbit around Sun-Earth Lagrange point L_2 since it allows the spacecraft to be oriented such that half of the celestial sphere is visible at all times, and the spacecraft may oppose the Sun, Earth, and Moon concurrently and at all times. This also leads to a very thermally stable environment. L_2 is near enough to Earth (roughly 1.5 million km) so that CDIM may communicate with ground stations without the Deep Space Network, and maintains near-constant communications geometry (Canalias *et al.*, 2004).

Around L_2, two types of orbit are considered: Lissajous and halo-type orbits. Lissajous orbits are quasi-periodic but may be smaller in radius than periodic halo orbits. Halo orbits are more costly to achieve in terms of delta-v, or energy to transfer into such trajectory. Station-keeping costs are not significantly

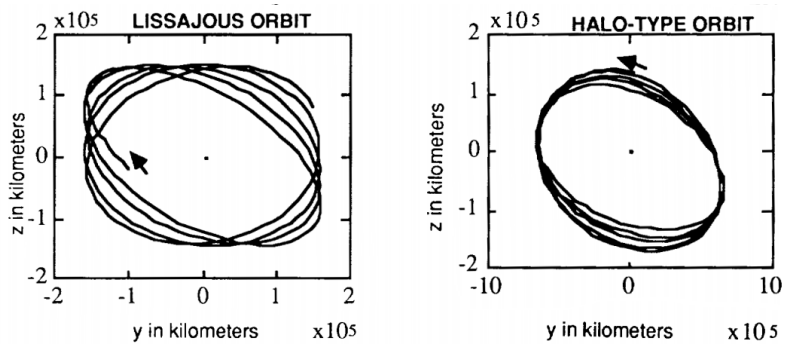

Fig. 5. *Left:* Orthographic view of a quasi-periodic Lissajous orbit. *Right:* Orthographic view of a periodic halo orbit. (Gordon, 1991)

different between the two orbits (Gordon, 1991). As such, CDIM may enter a Lissajous orbit around L_2 similar to the orbits of JWST and Herschel missions.

10. Launch Vehicle

CDIM will be comfortably within the mass and spatial limits of both currently available and development launch vehicles capable of delivering payloads to Sun-Earth Lagrange Point L_2. Future launch vehicles will be more than capable of delivering CDIM to L_2, and industry trends indicate that heavy and super-heavy vehicles will continue to come online by the time CDIM launches.

Due to the rigorous launch environment, deployable structures remain stowed until CDIM is delivered to a transfer orbit en route to L_2.

Table 5. Available launch vehicle configurations and their capabilities to send NASA payloads to L_2 (Rioux, 2016; Space Launch Report).

Vehicle	Payload to L_2	Fairing size	Cost†
Falcon 9 v1.1	2900 kg	5.2×13.1 m	\$97M
Falcon Heavy*	14 000 kg	5.2×13.1 m	\$120M
Atlas V 551	6100 kg	4.2×10.0 m	\$153M
		5.1×11.0 m	
Ariane V	6600 kg	5.4×12.7 m	\$165M
		5.4×13.8 m	
		5.4×17.0 m	\$220M
Delta IV Heavy	9800 kg	5.0×14.3 m	\$375M
		5.0×19.1 m	

† Launch costs may be higher due to NASA mandated oversight and testing.
* Costs and capacities are representative of design specifications for launch vehicles that are currently in development.

11. Cost Estimation

The overall cost of a space telescope may be broken down on the subsystem level. Each subsystem has its own set of cost drivers and uncertainties, but these subsystems may be analyzed on a high level as shares of a spacecraft's budget. Actual historical fiscal data, such as what is required for proper analysis,

is scarce. Estimations are made with engineering judgement based on available data along side single- and multi-variable parametric models.

To estimate the cost of the CDIM mission, costs are separated by subsystems which influence the *mission cost*, which includes hardware, development, ground support, integration, testing, science, and management. Existing generalized parametric cost estimation approaches identify key cost drivers for mission cost, but are based on prime contract costs which do not take NASA overhead costs into account (Stahl *et al.*, 2013; Bely, 2011). A more robust model for *total cost* shall include additional factors to account for these additional costs. Institutional overhead costs are assumed to add 50%, and labor costs add another 25%. An additional 30% funds shall be budgeted as reserves on top of all other mission and overhead costs to form a conservative estimate of CDIM's total cost.

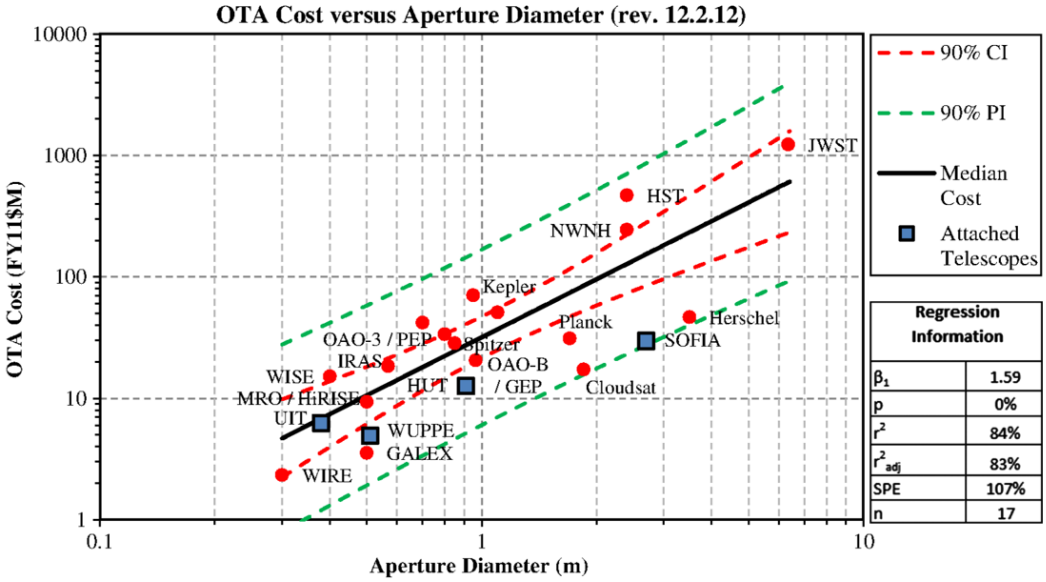

Fig. 6. Optical Telescope Assembly vs. cost correlation (Stahl *et al.*, 2013). Given a target OTA aperture diameter of 1.5 m for CDIM, a reasonable estimate of OTA cost is obtained from the median cost trendline.

Stahl *et al.* present an approach to estimating OTA cost based on correlations with data on flown space telescope missions. CDIM's projected costs may be obtained from these findings with engineering judgement, knowing that the data is drawn from a relatively small sample set. Thus, an OTA aperture diameter of 1.3 m yields a median OTA cost of \$48.0M and an OTA aperture diameter of 1.5 m yields a median OTA cost of \$58.2M.

Since OTA cost is found, estimates for other cost drivers may be obtained from relative cost values. As illustrated in Table 6, this estimate for the CDIM mission meets its \$850M target and remains under the \$1B cap for Probe-class missions.

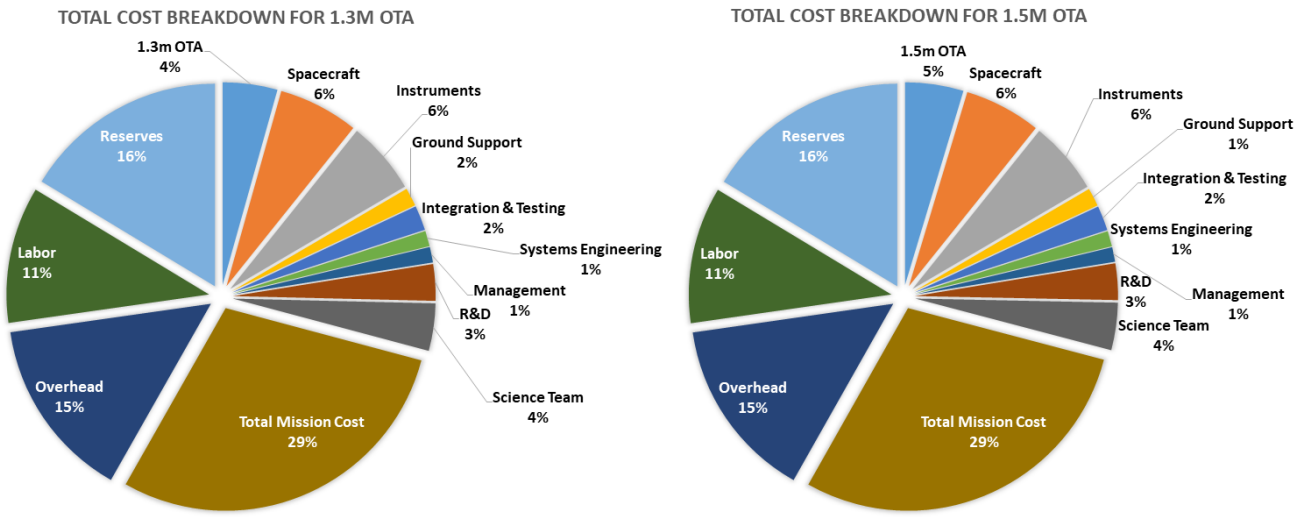

Fig. 7. CDIM estimated cost breakdown in percent of mission cost for a 1.3 m diameter OTA.

Driver	1.3 m OTA		1.5 m OTA	
OTA	15 %	$48.0M	16 %	$58.2M
Spacecraft	22 %	$70.4M	21 %	$76.4M
Instruments	20 %	$64.0M	20 %	$72.8M
Ground Support	5 %	$16.0M	5 %	$18.2M
Integration & Testing	7 %	$21.8M	7 %	$24.7M
Systems Engineering	4 %	$13.6M	4 %	$15.5M
Management	4 %	$13.6M	4 %	$14.6M
R&D	10 %	$32.0M	10 %	$36.4M
Science Team	13 %	$41.6M	13 %	$47.3M
Mission Cost		$320.0M		$363.8M
Overhead	+50%	$160.0M	+50%	$181.9M
Labor	+25%	$120.0M	+25%	$136.4M
Reserves	+30%	$180.0M	+30%	$204.6M
Total Cost		$780.0M		$886.6M

Table 6. CDIM total cost breakdown by subsystem.

12. Discussion

In this paper we describe the primary systems of the Cosmic Dawn Intensity Mapper space telescope at a high level to provide a baseline design for future development of the spacecraft. The CDIM mission is very early in development, and some science objectives and system requirements subject to further design trades. As such, this paper aims to be a baseline architecture rather than a complete spacecraft design study. Nevertheless, we show that a near-IR space telescope is feasible for a sub-$1B Probe-class NASA mission by using mature, proven technologies.

Acknowledgments

This research was completed to fulfill the requirements of the Rochester Institute of Technology Kate Gleason College of Engineering Bachelor of Science/Master of Engineering Dual-Degree program with support from the RIT College of Science Center for Detectors. The authors thank all those who spent some of their brainpower thinking about CDIM, especially Dr. Asantha Cooray (U.C. Irvine) and all members of the CDIM science team, and other RIT faculty members. Special thanks to Chi H. Nguyen (RIT), Steve Unwin (NASA JPL), and all authors and editors of *Space Mission Engineering:The New SMAD*.

References

Bard, S. [1987] *Journal of Spacecraft and Rockets* **24**, 193, doi:10.2514/3.25898.

Bely, P.-Y. [2011] *The Design and Construction of Large Optical Telescopes* (Springer).

Canalias, E., Gomez, G., Marcote, M. & Masdemont, J. [2004] *ESA Advanced Concept Team* .

Cooray, A., Bock, J., Burgarella, D., Chary, R., Chang, T.-C., Doré, O., Fazio, G., Ferrara, A., Gong, Y., Santos, M., Silva, M. & Zemcov, M. [2016] *ArXiv e-prints* .

Couto, P., Mantelli, M. B. H., Marotta, E. E. & Fuller, J. J. [2002] *Journal of Thermophysics and Heat Transfer* **16**, 313âĂŞ323, doi:10.2514/2.6708.

Doré, O., Bock, J., Capak, P., de Putter, R., Eifler, T., Hirata, C., Korngut, P., Krause, E., Masters, D., Raccanelli, A. *et al.* [2014] *arXiv preprint arXiv:1412.4872* .

Evans, S. W. *et al.* [2002] *Next Generation Space Telescope Program, NASA Marshall Space Flight Center, MSFC, AL, http://sail. msfc. nasa. gov/nse/sgst. html* .

Gardner, J. P., Mather, J. C., Clampin, M., Doyon, R., Greenhouse, M. A., Hammel, H. B., Hutchings, J. B., Jakobsen, P., Lilly, S. J., Long, K. S., Lunine, J. I., Mccaughrean, M. J., Mountain, M., Nella, J., Rieke, G. H., Rieke, M. J., Rix, H.-W., Smith, E. P., Sonneborn, G., Stiavelli, M., Stockman, H. S., Windhorst, R. A. & Wright, G. S. [2006] *Space Science Reviews* **123**, 485, doi:10.1007/s11214-006-8315-7, URL http://dx.doi.org/10.1007/s11214-006-8315-7.

Gilmore, D. & Donabedian, M. [2003] *Spacecraft Thermal Control Handbook: Cryogenics*, Spacecraft Thermal Control Handbook (Aerospace Press), ISBN 9781884989148, URL https://books.google.com/books?id=x5NTAAAAMAAJ.

Gordon, S. C. [1991] "Orbit determination error analysis and station-keeping for liberation point trajectories," PhD thesis, Purdue Univ., West Lafayette, IN.

Green, J., Schechter, P., Baltay, C., Bean, R., Bennett, D., Brown, R., Conselice, C., Donahue, M., Fan, X., Gaudi, B. S., Hirata, C., Kalirai, J., Lauer, T., Nichol, B., Padmanabhan, N., Perlmutter, S., Rauscher, B., Rhodes, J., Roellig, T., Stern, D., Sumi, T., Tanner, A., Wang, Y., Weinberg, D., Wright, E., Gehrels, N., Sambruna, R., Traub, W., Anderson, J., Cook, K., Garnavich, P., Hillenbrand, L., Ivezic, Z., Kerins, E., Lunine, J., McDonald, P., Penny, M., Phillips, M., Rieke, G., Riess, A., van der Marel, R., Barry, R. K., Cheng, E., Content, D., Cutri, R., Goullioud, R., Grady, K., Helou, G., Jackson, C., Kruk, J., Melton, M., Peddie, C., Rioux, N. & Seiffert, M. [2012] "Wide-field infrared survey telescope (wfirst) final report," .

Morgante, G., Terenzi, L., Eccleston, P., Bradshaw, T., Crook, M., Linder, M., Hunt, T., Winter, B., Focardi, M., Malaguti, G. & et al. [2015] *EChO - Exoplanet Characterisation Observatory* , 387âĂŞ416doi:10.1007/978-94-024-0837-9_22.

Rasbach, C. [1988] *26th Aerospace Sciences Meeting* doi:10.2514/6.1988-557.

Rioux, N. [2016] "Getting to orbit: Launch vehicles," .

Ross, R. [2005] *Cryocoolers 13* (Springer US), ISBN 9780387239019, URL https://books.google.com/books?id=ZbxTAAAAMAAJ.

Space Launch Report [2017] "Launch vehicle datasheets," http://www.spacelaunchreport.com/.

Stahl, H. P., Henrichs, T., Luedtke, A. & West, M. [2013] *Optical Engineering* **52**, 091805, doi:10.1117/1.OE.52.9.091805, URL http://dx.doi.org/10.1117/1.OE.52.9.091805.

Turner, T., Baltz, E. & Kirschner, R. [2016] "For compactness and ruggedness, linear variable filters fit the bill," URL https://www.photonics.com/Article.aspx?AID=60941.

Wertz, J. R., Everett, D. F. & Puschell, J. J. [2015] *Space mission engineering: the new SMAD* (Microcosm Press).

Wiseman, J., Clampin, M., Danchi, W., Mather, J., Oegerle, W., Barry, R., Traub, W., Stapelfeldt, K., Lissauer, J., Borucki, W., Greene, T., Bennett, D. & Johnston, K. [2015] "Space-based "probe class" missions for exoplanet research," https://science.gsfc.nasa.gov/667/whitepapers/ProbeClassMissions_whitepaper.pdf.

Zemcov, M., Crill, B., Ryan, M. & Staniszewski, Z. [2016] doi:10.1142/S2251171716500070.